Nonlinear pumping induced multipartite entanglement in a hybrid magnon cavity QED system

Y. Zhou,[1,2] S. Y. Xie,[1,*] C. J. Zhu,[3,4,†] and Y. P. Yang[1,‡]

[1]*MOE Key Laboratory of Advanced Micro-Structured Materials, School of Physics Science and Engineering, Tongji University, Shanghai 200092, China*

[2]*School of Electronics and Information Engineering, Taizhou University, Taizhou 318000, China*

[3]*School of Physical Science and Technology, Soochow University, Suzhou 215006, China*

[4]*Collaborative Innovation Center of Light Manipulations and Applications, Shandong Normal University, Jinan 250358, China*

(Received 29 June 2022; revised 21 September 2022; accepted 14 November 2022; published 6 December 2022)

We present a proposal to produce bipartite and tripartite entanglement in a hybrid magnon cavity QED system. Two macroscopic yttrium iron garnet (YIG) spheres are coupled to a single-mode microwave cavity, where the cavity photons are generated via a two-photon process induced by a strong pump field. Using mean-field theory, we show that nonlinear pumping can result in strong bipartite entanglement between the cavity photon and magnon under two conditions, i.e., $\delta_c\delta_m = 2g^2$ and $\delta_c = -\delta_m$. For the latter one, we also show the possibility for producing bipartite entanglement between two magnon modes as well as tripartite entanglement among three modes. Combining these two conditions, we further derive a third condition, i.e., $\delta_m^2 - \phi^2 + 2g^2 = 0$, where tripartite entanglement can be achieved when two magnon modes have different resonant frequencies.

DOI: 10.1103/PhysRevB.106.224404

I. INTRODUCTION

Yttrium iron garnet (YIG) materials are good candidates for demonstrating interesting phenomena in quantum optics and the condensed matter field of magnetism due to their high Curie temperature, high spin density, low dissipation rate, and good tunability [1,2]. Particularly, ferromagnetic resonance (FMR) induced collective spin dynamics gives rise to a new research field of magnonics by combining meso- and nanoscale science. With modern lithography and sensing techniques, a great amount of fascinating phenomena have been reported theoretically and experimentally, including the dynamics of skyrmions [3], magnetic vortices [4,5], the spin pumping effect [6–9], and so on. All these properties would enable further investigations of quantum optical phenomena in hybrid quantum systems, integrating magnonic systems with photons [10,11], qubits [12–14], optomechanics [15–17], and others.

In addition, the interaction between an ensemble of spins and the cavity field plays an important role in the development of novel hybrid quantum systems. In the field of quantum magnonics, photons confined to a cavity mode interact more strongly with a matter polarization, producing the cavity magnon polariton as a new type of quasiparticle [18,19]. This is because magnon polaritons have a spin density many orders of magnitude higher than ensembles consisting of atoms, molecules, nitrogen vacancy centers, ion doped crystals, and so on. Notably, strong coupling between a Kittel mode in a YIG sphere and the photonic mode has been observed at room temperature [20–23].

Recently, this subfield of cavity electromagnonics involving the interaction between magnon modes and the cavity light mode has developed rapidly. Many emergent phenomena have been found, such as cavity spintronics [24–26], bistability [27–29], magnon dark modes [22,30], magnetically controllable slow light [31,32], and magnon induced transparency [33,34]. Particularly, the preparation of entangled states in ferromagnetic materials, e.g., YIG spheres, has attracted much attention. Several methods have been proposed theoretically to realize bipartite and tripartite entanglements [15,35–38]. Other applications have also been reported such as the generation of squeezed states of magnons and phonons in cavity magnomechanics [39], and the implementation of nonreciprocal transmission for a microwave field [40].

In this paper, we present a method to produce bipartite and tripartite entanglements in a two-YIG-sphere cavity QED system via the nonlinear pumping process, which can be implemented by utilizing nonlinear materials [41–45], photonic waveguide systems [46,47], as well as the dynamical Casimir effect demonstrated in optomechanics systems [48–51]. We first consider a special case where two magnon modes have the same resonant frequencies. Then, we obtain two conditions for realizing photon-magnon entanglement, and magnon-magnon entanglement. Moreover, tripartite entanglement among the cavity field and two magnon modes can also be achieved under one of these two conditions. Then, we consider the case where two magnon modes have different resonant frequencies. We show that a different condition for the implementation of tripartite entanglement among three modes can be easily derived. We also show that nonlinear pumping can result in a strong gain of cavity photon numbers, and further enhance the interaction strength between

*Corresponding author: xieshuangyuan@tongji.edu.cn
†Corresponding author: cjzhu@suda.edu.cn
‡Corresponding author: yaping_yang@tongji.edu.cn

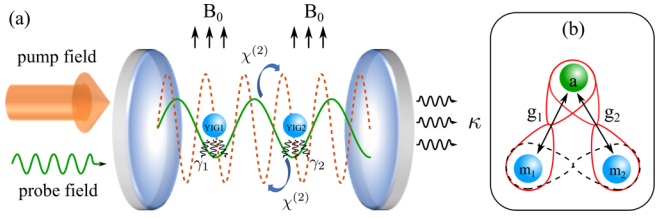

FIG. 1. (a) Schematic of a hybrid magnon cavity QED system. Two YIG spheres with resonant frequencies ω_{m_1} and ω_{m_2} are located inside a microwave cavity driven by a pump field and an auxiliary probe field ε_p. The pump field photons are transferred to the probe field photons via a two-photon process with nonlinear interaction strength Ω. Here, γ_1 and γ_2 denote the decay rates of two magnon modes, while κ denotes the decay rate of the cavity mode. (b) Interactions among the subsystems. Two magnon modes linearly couple to the cavity mode with coupling strengths g_1 and g_2, respectively. The nonlinear interaction results in bipartite entanglements between two magnon modes and the cavity mode, respectively. With some specific conditions, two magnon modes can be entangled, which further leads to tripartite entanglements.

photons and magnons, yielding entanglements with weak nonlinearity.

II. THEORETICAL MODEL

As shown in Fig. 1, we consider a magnon-photon hybrid system where two YIG spheres are placed in a single-mode microwave cavity with resonant frequency ω_c. With current experimental techniques, strong couplings between the cavity photons and collective spin excitations in YIG spheres can be achieved [52–55]. In our system, we only take into account the Kittel modes which have a spatially uniform profile and are subject to giant magnetic moments, i.e., $\mathbf{M}_j = \gamma \mathbf{S}^{(j)}/V$. Here, $\gamma = e/m_e c$ is the gyromagnetic ratio for electron spin and $\mathbf{S}^{(j)}$ $(j = 1, 2)$ denotes the collective spin operator of the jth YIG sphere, which couples the external magnetic field and the magnetic field inside the cavity. Thus, the frequency of the Kittel mode in the jth YIG sphere $\omega_{m_j} = \gamma H_z^{(j)}$, which can be flexibly tuned by adjusting the external magnetic field. By means of the Holstein-Primakoff (HP) transform [56], the collective spin operators can be approximately represented by the boson creation and annihilation operators ($\hat{m}_j^\dagger$ and $\hat{m}_j$) with $[\hat{m}_j, \hat{m}_j^\dagger] = 1$. Then, the raising and lowering operators of the spin can be approximately expressed as $\hat{m}_j \approx \hat{S}_+^{(j)}/\sqrt{(2S)}$ and $\hat{m}_j^\dagger \approx \hat{S}_-^{(j)}/\sqrt{(2S)}$ with $\hat{S}_\pm^{(j)} = \sum_{j=1}^{N} \hat{\sigma}_\pm^{(j,N)}$ and $S = Ns$ being the total spin number of the corresponding collective spin operator, with the total number of spins $N = \rho V$ and the spin number $s = 5/2$. Here, we consider a typical yttrium iron garnet with high spin density $\rho = 4.22 \times 10^{27}$ m^{-3} and diameter $d = 1$ mm [27,57]. The cavity is driven by a weak probe field with resonant frequency ω_p and a pump field with resonant frequency $\omega_P = 2\omega_p$. We must point out that the probe field is just used to obtain the conditions for the implementation of entanglements, which is not essential in experiments.

Under the rotating-wave approximation in the frame of the probe field, the Hamiltonian of this magnon cavity system shown in Fig. 1 is (setting $\hbar = 1$)

$$\hat{H} = \delta_c \hat{a}^\dagger \hat{a} + \sum_{j=1,2} [\delta_{m_j} \hat{m}_j^\dagger \hat{m}_j + g_j (\hat{a}\hat{m}_j^\dagger + \hat{a}^\dagger \hat{m}_j)] + \Omega(\hat{a}^2 + \hat{a}^{\dagger 2}) + \varepsilon_p(\hat{a} + \hat{a}^\dagger), \tag{1}$$

where $\hat{a}$ ($\hat{a}^\dagger$) denotes the annihilation (creation) operator of the cavity mode, $\delta_c = \omega_c - \omega_p$ and $\delta_{m_j} = \omega_{m_j} - \omega_p$. $g_j \propto (\gamma/2)\sqrt{2Ns\hbar\omega_c\mu_0/V_c}$ describes the magnon cavity coupling strength [10], where μ_0 is the vacuum permeability, and V_c is the mode volume of the microwave cavity. ε_p is the driving strength of the probe field, and the cavity photons also interact with a strong pump field via a two-photon process with nonlinear interaction strength Ω [58,59]. Such a kind of nonlinear pumping can be implemented in various quantum systems [41–51], e.g., a resonator with lithium niobate or aluminum nitride [60].

The dynamics of this coupled system is described by the quantum master equation, which reads

$$\frac{d\hat{\rho}}{dt} = -i[\hat{H}, \hat{\rho}] + \frac{\kappa}{2}\hat{\mathcal{L}}_\kappa[\hat{\rho}] + \sum_{j=1,2} \frac{\gamma_j}{2}\hat{\mathcal{L}}_\gamma^{(j)}[\hat{\rho}], \tag{2}$$

where $\hat{\rho}$ is the density matrix of the system. The decay terms are given by $\hat{\mathcal{L}}_\kappa[\hat{\rho}] = 2\hat{a}\hat{\rho}\hat{a}^\dagger - \hat{a}^\dagger\hat{a}\hat{\rho} - \hat{\rho}\hat{a}^\dagger\hat{a}$ and $\hat{\mathcal{L}}_\gamma^{(j)}[\hat{\rho}] = 2\hat{m}_j\hat{\rho}\hat{m}_j^\dagger - \hat{m}_j^\dagger\hat{m}_j\hat{\rho} - \hat{\rho}\hat{m}_j^\dagger\hat{m}_j$ with the cavity decay rate κ and magnon decay rate γ_j, respectively.

Then, the time evolution of the bosonic operators, including the thermal fluctuation about the mean values, can be described by the quantum Langevin equations (QLEs), which read

$$\frac{d\hat{a}}{dt} = -i(\delta_c - i\kappa)\hat{a} - ig_1\hat{m}_1 - ig_2\hat{m}_2 - i\varepsilon_p - 2i\Omega\hat{a}^\dagger + \sqrt{2\kappa}\hat{a}^{\text{in}}, \tag{3}$$

$$\frac{d\hat{m}_1}{dt} = -i(\delta_{m_1} - i\gamma_1)\hat{m}_1 - ig_1\hat{a} + \sqrt{2\gamma_1}\hat{m}_1^{\text{in}}, \tag{4}$$

$$\frac{d\hat{m}_2}{dt} = -i(\delta_{m_2} - i\gamma_2)\hat{m}_2 - ig_2\hat{a} + \sqrt{2\gamma_2}\hat{m}_2^{\text{in}}, \tag{5}$$

where $\hat{a}^{\text{in}}$ and $\hat{m}_j^{\text{in}}$ $(j = 1, 2)$ denote input quantum noises of the cavity mode and the jth magnon mode, respectively. They obey the following correlations [61]: $\langle \hat{a}^{\text{in}}(t)\hat{a}^{\text{in}\dagger}(t')\rangle = \delta(t - t')$, $\langle \hat{a}^{\text{in}\dagger}(t)\hat{a}^{\text{in}}(t')\rangle = 0$, $\langle \hat{m}_j^{\text{in}}(t)\hat{m}_j^{\text{in}\dagger}(t')\rangle = \delta(t - t')$, $\langle \hat{m}_j^{\text{in}\dagger}(t)\hat{m}_j^{\text{in}}(t')\rangle = 0$. In the following, we set $g_1 = g_2 \equiv g$, $\gamma_1 = \gamma_2 \equiv \gamma_0$ for mathematical simplicity. Generally, Eqs. (3)–(5) can be solved by using the mean-field approximation, i.e., setting an arbitrary operator $\hat{o} = o + \delta\hat{o}$ $(o = a, m_1, m_2)$. Here, $o \equiv \langle \hat{o} \rangle = \text{Tr}(\hat{\rho}\hat{o})$ denotes the average value of the operator $\hat{o}$, while $\delta\hat{o}$ represents the quantum fluctuation about the average value.

To show the physical mechanism of the entanglement more clearly, we first set $\omega_{m_1} = \omega_{m_2} \equiv \omega_m$. Under the steady-state approximation, Eqs. (3)–(5) can be linearized, yielding

$$(\delta_c - i\kappa)a + g(m_1 + m_2) + 2\Omega a^* = -\varepsilon_p, \tag{6}$$

$$(\delta_m - i\gamma_0)m_j + ga = 0, \tag{7}$$

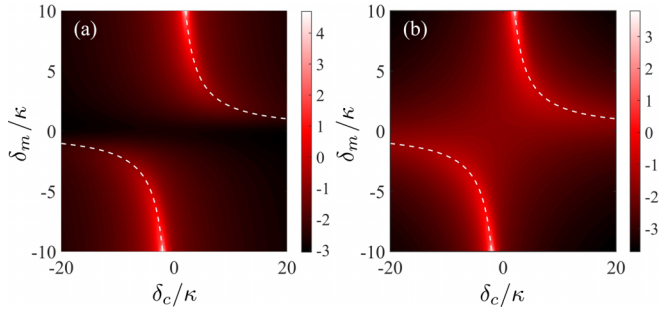

FIG. 2. Average photon number n_c [(a)] and magnon excitation number $n_{m_1}(n_{m_2})$ [(b)] on a logarithmic scale as functions of normalized detunings δ_c/κ and δ_m/κ. Here, the white dashed curves indicate the condition $\delta_c\delta_m = 2g^2$ where a maximum value of the average photon number and magnon excitation number can be observed. System parameters are given in the text.

where $j = 1, 2$ and $\delta_m = \omega_m - \omega_p$. The solutions of the above equations are given by

$$a = \frac{\varepsilon_p}{4\Omega^2 - |D_0|^2}(D_0^* - 2\Omega), \tag{8a}$$

$$m_1 = m_2 = -ga/\delta_m, \tag{8b}$$

where $D_0 = \Delta_c - 2g^2/\Delta_m$ with complex detuning $\Delta_c = \delta_c - i\kappa$ and $\Delta_m = \delta_m - i\gamma_0$. Then, one can easily obtain the average photon number $n_c \equiv \langle a^\dagger a\rangle \approx |a|^2$ and the magnon excitation numbers of the jth YIG sphere $n_{m_j} \equiv \langle m_j^\dagger m_j\rangle \approx |m_j|^2$. In view of Eq. (8a) and dropping all decay terms, it is noted that the cavity photons can be excited with their maximal efficiency if the condition

$$\delta_c\delta_m = 2g^2 \tag{9}$$

is satisfied. Simultaneously, the magnon excitation number will also reach its maximum. In Fig. 2, we show the average photon number n_c [Fig. 2(a)] and the magnon excitation number n_{m_1} (n_{m_2}) in the first (second) YIG sphere [Fig. 2(b)] on a logarithmic scale as functions of the detunings δ_c and δ_m, respectively. Here, we choose $\varepsilon_p = \kappa$ and the nonlinear interaction strength $\Omega/\kappa = 0.6$, $\gamma_0 = \kappa$, $g/\kappa = 3.2$, which are feasible with current experiments [10,62]. In Fig. 2(a), it is clear to see that there exist two excitation branches in the cavity excitation spectrum with the condition $\delta_c\delta_m = 2g^2$. As shown in Fig. 2(b), similar characteristics can be observed in the magnon excitation spectrum. We must point out that the maximal value of the magnon excitation numbers is just about 10^3 so that the weak excitation assumption $m_1, m_2 \ll 2Ns$ is satisfied and the HP approximation is valid. In the following, we will show how such a weak magnon excitation can lead to entanglement between cavity photons and magnons in both YIG spheres.

III. BIPARTITE ENTANGLEMENT

First, let us consider bipartite entanglement between cavity photons and magnons by studying the properties of the quadrature fluctuations of the cavity field and the magnon modes, which are defined as $\delta X = (\delta\hat{a} + \delta\hat{a}^\dagger)/\sqrt{2}$, $\delta Y = i(\delta\hat{a}^\dagger - \delta\hat{a})/\sqrt{2}$, $\delta x_1 = (\delta\hat{m}_1 + \delta\hat{m}_1^\dagger)/\sqrt{2}$, $\delta y_1 = i(\delta\hat{m}_1^\dagger - \delta\hat{m}_1)/\sqrt{2}$, $\delta x_2 = (\delta\hat{m}_2 + \delta\hat{m}_2^\dagger)/\sqrt{2}$, and $\delta y_2 = i(\delta\hat{m}_2^\dagger - \delta\hat{m}_2)/\sqrt{2}$. Neglecting higher-order fluctuations of the operators, the evolution of quadrature fluctuations can be described by the linearized QLEs, which read

$$\dot{f}(t) = Af(t) + \eta, \tag{10}$$

where $f(t) = [\delta X(t), \delta Y(t), \delta x_1(t), \delta y_1(t), \delta x_2(t), \delta y_2(t)]^{\mathrm{T}}$, and $\eta(t) = [\sqrt{2\kappa}X^{\mathrm{in}}, \sqrt{2\kappa}Y^{\mathrm{in}}, \sqrt{2\gamma_0}x_1^{\mathrm{in}}, \sqrt{2\gamma_0}y_1^{\mathrm{in}}, \sqrt{2\gamma_0}x_2^{\mathrm{in}}, \sqrt{2\gamma_0}y_2^{\mathrm{in}}]^{\mathrm{T}}$ is a vector denoting the input noises. The drift matrix is defined as

$$A = \begin{pmatrix} -\kappa & \delta_c - 2\Omega & 0 & g & 0 & g \\ -\delta_c - 2\Omega & -\kappa & -g & 0 & -g & 0 \\ 0 & g & -\gamma_0 & \delta_m & 0 & 0 \\ -g & 0 & -\delta_m & -\gamma_0 & 0 & 0 \\ 0 & g & 0 & 0 & -\gamma_0 & \delta_m \\ -g & 0 & 0 & 0 & -\delta_m & -\gamma_0 \end{pmatrix}. \tag{11}$$

For such a system, a 6×6 covariance matrix (CM) $\mathcal{V}$ can be used to describe a continuous variable three-mode Gaussian state. The corresponding element of this CM is defined as $\mathcal{V}_{ij} = \langle f_i(t)f_j(t') + f_j(t')f_i(t)\rangle/2$ ($i, j = 1, 2, \ldots, 6$). Generally, we can solve the Lyapunov equation to obtain the steady-state CM $\mathcal{V}$ [63,64], i.e.,

$$A\mathcal{V} + \mathcal{V}A^T = -D, \tag{12}$$

where D is a 6×6 diffusion matrix with $D_{ij}\delta(t - t') = \langle \eta_i(t)\eta_j(t') + \eta_j(t')\eta_i(t)\rangle/2$. Then, we calculate the logarithmic negativity [65,66] to quantitatively measure the bipartite entanglement $E_{\alpha\beta}$ ($\alpha, \beta = a, m_1, m_2$) between any two different modes, i.e.,

$$E_{\alpha\beta} \equiv \max\{0, -\ln 2\tilde{\nu}_-\}, \tag{13}$$

where $\tilde{\nu}_- = \min\{\mathrm{eig}(i\Omega_2\tilde{\mathcal{V}}_4)\}$ with $\tilde{\mathcal{V}}_4 = P_{1|2}\mathcal{V}_4P_{1|2}$. Here, $\Omega_2 = \oplus_{j=1}^2 i\sigma_y$, $P_{1|2} = \sigma_z \oplus I$, and $\mathcal{V}_4$ is a 4×4 CM of two arbitrary subsystems in this three-mode system, which can be obtained by deleting rows and columns of irrelevant modes in CM $\mathcal{V}$. σ_y and σ_z are the Pauli matrices. As usual, $E_{\alpha\beta} > 0$ denotes the existence of bipartite entanglement. Figure 3(a) shows the bipartite entanglement E_{am_1} (E_{am_2}) between the magnon mode in the first (second) YIG sphere and the cavity mode as functions of the detunings δ_c and δ_m, respectively. The system parameters are the same as those used in Fig. 2. Obviously, strong bipartite entanglements between the magnon mode and the cavity mode occur under two different conditions. One is $\delta_c\delta_m = 2g^2$ (white dashed curves) as demonstrated in Fig. 2. The other (white solid line) is

$$\delta_c = -\delta_m, \tag{14}$$

which can be understood by exploring the system in a bare state picture. Considering two bare states labeled by $|N_c, N_{m_j}\rangle$ and $|N_c - 1, N_{m_j} + 1\rangle$, a bipartite entanglement state such as $(|N_c, N_{m_1}\rangle + |N_c - 1, N_{m_1} + 1\rangle)/\sqrt{2}$ will be produced if both states have the same excitation probabilities. Thus, the probe field frequency must satisfy $\omega_p = (\omega_c + \omega_{m_j})/2$, yielding $\delta_c = -\delta_m$. It is also noted that, in a small regime near $\delta_c = \delta_m = 0$ (i.e., $\omega_c = \omega_{m_1} = \omega_{m_2}$), the photon mode and magnon mode are not entangled and $E_{am_1} = E_{am_2} = 0$ since these two states cannot be distinguished [see Fig. 3(a)].

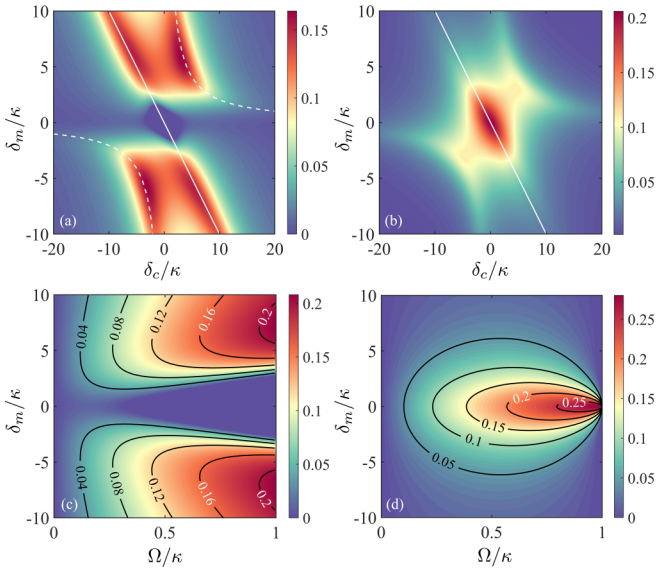

FIG. 3. Density plot of bipartite entanglement $E_{am_1} = E_{am_2}$ [(a)] and $E_{m_1m_2}$ [(b)] vs normalized detunings δ_c/κ and δ_m/κ. White dashed curves indicate the condition $\delta_c\delta_m = 2g^2$, while white solid lines indicate the condition $\delta_c = -\delta_m$. (c) and (d) show the density plot of bipartite entanglements $E_{am_1} = E_{am_2}$ and $E_{m_1m_2}$ against the normalized nonlinear interaction strength Ω/κ and detuning δ_m/κ by fixing $\delta_c = -\delta_m$.

In Fig. 3(b), we show the bipartite entanglement $E_{m_1m_2}$ between two magnon modes. In contrast to the bipartite entanglement E_{am_j} between photons and magnons, the bipartite entanglement $E_{m_1m_2}$ only appears in the regime near the condition of $\delta_c = -\delta_{m_1}$. In particular, maximal bipartite entanglement between two magnon modes occurs at the center point with $\omega_c = \omega_{m_1} = \omega_{m_2}$. However, at this point, the magnon mode and cavity mode are not entangled.

Here, we must point out that nonlinear pumping is the key for generating bipartite entanglements. To show this point, we fix $\delta_c = -\delta_m$. Figures 3(c) and 3(d) show E_{am_1} (E_{am_2}) and $E_{m_1m_2}$ against the normalized detuning δ_m/κ and nonlinear interaction strength Ω/κ, respectively. Obviously, $E_{am_1} = E_{am_2} = E_{m_1m_2} = 0$ (nonentanglement) if the nonlinear interaction strength $\Omega = 0$. Bipartite entanglements E_{am_1} (E_{am_2}) and $E_{m_1m_2}$ are significantly enhanced as the nonlinear interaction strength Ω increases. It is noted that these nonlinearity induced bipartite entanglements reach up to 0.1 even for a weak nonlinear interaction strength, e.g., $\Omega/\kappa = 0.5$. It is as strong as the phonon induced bipartite entanglements reported in Ref. [67], where the average magnon excitation number is above 10^7 to acquire a strong nonlinear effect. Compared with Figs. 3(c) and 3(d), we notice that it is possible to find some regimes where mutual bipartite entanglements (i.e., tripartite entanglement with nonzero E_{am_1}, E_{am_2}, and $E_{m_1m_2}$) can be achieved when the driving field is detuned.

IV. TRIPARTITE ENTANGLEMENT

To verify this feature, we adopt the minimum residual contangle as a bona fide quantification of tripartite entanglement [68,69]. Here, contangle is a CM analog of tangle for discrete-variable tripartite entanglement, and the minimum residual contangle is given by

$$R_\tau^{\min} \equiv \min\{R_\tau^{a|m_1m_2}, R_\tau^{m_1|am_2}, R_\tau^{m_2|am_1}\}, \tag{15}$$

where $R_\tau^{i|jk} \equiv C_{i|jk} - C_{i|j} - C_{i|k} \geqslant 0$ $(i, j, k = a, m_1, m_2)$ denotes the residual contangle with $C_{u|v}$ being the contangle of subsystems u and v (v can contain one or two modes). Here, we consider that v contains two modes, and the contangle $C_{i|jk} = [\max\{0, -\ln(2\tilde{\nu}_-)\}]^2$, where $\tilde{\nu}_- \equiv \min\{\mathrm{eig}(i\Omega_3\tilde{\mathcal{V}}_6)\}$ with $\Omega_3 = \oplus_{j=1}^3 i\sigma_y$ and $\tilde{\mathcal{V}}_6 = P_{i|jk}\mathcal{V}P_{i|jk}$. Here, $P_{1|23} = \sigma_z \oplus I \oplus I$, $P_{2|13} = I \oplus \sigma_z \oplus I$, and $P_{3|12} = I \oplus I \oplus \sigma_z$ denote partial transposition matrices. Thus, $R_\tau^{\min} > 0$ represents the existence of genuine tripartite entanglement in the system.

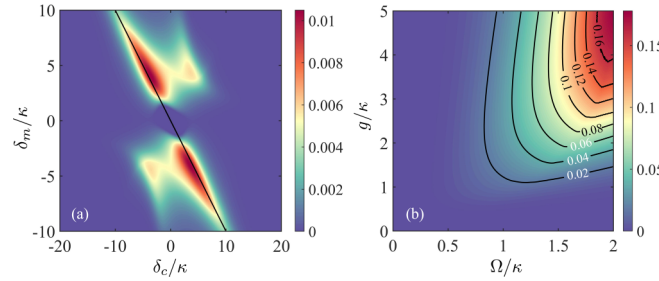

FIG. 4. (a) Tripartite entanglement $R_\tau^{\min}$ vs normalized detunings δ_c/κ and δ_m/κ. The black solid line indicates the condition $\delta_c = -\delta_m$. (b) Maximal tripartite entanglement $R_\tau^{\min}$ is plotted as functions of the normalized nonlinear interaction strength Ω/κ and coupling strength g/κ by fixing $\delta_c = -\delta_m$ and scanning magnon detuning δ_m over a wide range.

Next, we will discuss the possibility for generating a tripartite entanglement among three modes. In Fig. 4(a), we show the tripartite entanglement $R_\tau^{\min}$ versus detunings δ_c and δ_m, respectively. Here, the system parameters are the same as those used in Fig. 2, and the black solid line indicates the condition $\delta_c = -\delta_m$. As expected, tripartite entanglements occur near this condition with nonzero cavity/magnon detuning. Figure 4(b) shows more clearly the presence of tripartite entanglement by setting $\delta_c = -\delta_m$. Here, we plot maximal tripartite entanglement against the normalized coupling strength g/κ and the nonlinear interaction strength Ω/κ by scanning the magnon detuning δ_m over a wide range. Obviously, tripartite entanglement can be produced when a set of suitable photon-magnon interaction strength g and nonlinear interaction strength Ω is chosen.

Finally, let us study the presence of tripartite entanglements when two magnon modes have different resonant frequencies. To show the properties of tripartite features more clearly, we define the average magnon frequency $\bar{\omega}_m = (\omega_{m_1} + \omega_{m_2})/2$ and the frequency difference $\phi = (\omega_{m_1} - \omega_{m_2})/2$. Then, the detunings are given by $\delta_{m_1} = \delta_m + \phi$ and $\delta_{m_2} = \delta_m - \phi$ with $\delta_m = \bar{\omega}_m - \omega_p$. Based on the above analysis, it is found that there exist two different conditions to realize strong bipartite entanglement between the photon mode and single magnon mode [see Eqs. (8)]. Therefore, the presence of tripartite entanglement with two different magnon modes can be predicted if the frequency of the first magnon mode satisfies $\delta_c = -\delta_{m_1}$, while the frequency of the second magnon mode satisfies $\delta_c\delta_{m_2} = 2g^2$ simultaneously. Combining these two conditions,

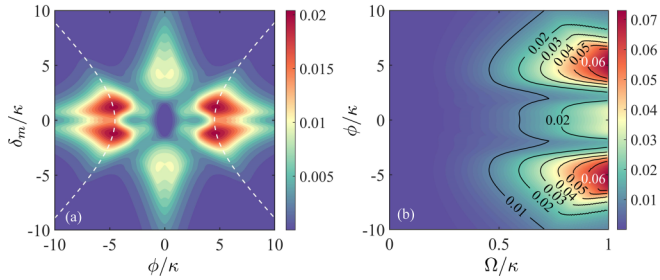

FIG. 5. (a) Tripartite entanglement $R_\tau^{\min}$ vs the frequency difference between two magnon modes ϕ/κ and the detuning δ_m/κ. Here, we choose $\delta_c = -\delta_m$ and white dashed curves indicate the condition $\delta_m^2 - \phi^2 + 2g^2 = 0$. (b) Maximal tripartite entanglement $R_\tau^{\min}$ vs the nonlinear interaction strength Ω/κ and the frequency difference between two magnon modes ϕ/κ by setting $\delta_m^2 - \phi^2 + 2g^2 = 0$ and scanning the detuning δ_m over a wide range.

one can easily obtain

$$\delta_m^2 - \phi^2 + 2g^2 = 0 \tag{16}$$

for achieving strong tripartite entanglement. To verify this prediction, we plot $R_\tau^{\min}$ versus the average magnon frequency detunings δ_m and magnon frequency deviation ϕ [70] in Fig. 5(a). Here, we set $\delta_c = -\delta_m$ and other system parameters are the same as those used in Fig. 2. It is clear to see that maximal tripartite entanglements appear at the condition $\delta_m^2 - \phi^2 + 2g^2 = 0$ indicated by the white dashed curves. In Fig. 5(b), we show the influence of the nonlinear interaction strength Ω on the presence and quality of tripartite entanglement. Here, we plot optimal tripartite entanglement versus ϕ/κ and Ω/κ by scanning the detuning δ_m over a wide range. It is found that tripartite entanglement with two different magnon modes can also be realized under a weak nonlinear interaction and it can be significantly enhanced as the nonlinear interaction strength Ω increases.

V. CONCLUSION

In conclusion, we have proposed a scheme to generate bipartite and tripartite entanglements in a hybrid magnon cavity QED system, where the cavity photons are generated via the two-photon process. In the presence of nonlinear pumping, we show that bipartite entanglement between the cavity mode and magnon mode can be achieved under two conditions. One is $\delta_c\delta_m = 2g^2$, and the other is $\delta_c = -\delta_m$. For the second condition, it is also possible to produce mutual entanglement between two magnon modes near the resonance region. In addition, we show that optimal tripartite entanglement can be implemented if the second condition $\delta_c = -\delta_m$ is fulfilled. Combining these two conditions, we derive a third condition for realizing tripartite entanglement among the photon mode and two magnon modes with different resonant frequencies, i.e., $\delta_m^2 - \phi^2 + 2g^2 = 0$. All these conditions are helpful for experimentalists to realize macroscopic bipartite and tripartite entanglements in hybrid magnon cavity QED systems.

ACKNOWLEDGMENTS

We thank Dr. Jie Li at Zhejiang University for helpful discussions. This work has been supported by the National Natural Science Foundation of China (Grants No. 61975154 and No. 12274326) and the National Key Research and Development Program of China (Grants No. 2021YFA1400600 and No. 2021YFA1400602).

[1] B. Bhoi and S. K. Kim, Roadmap for photon-magnon coupling and its applications, Solid State Phys. **71**, 39 (2020).
[2] M. Harder and C. M. Hu, Cavity spintronics: An early review of recent progress in the study of magnon–photon level repulsion, Solid State Phys. **69**, 47 (2018).
[3] X. Wang, L. Chotorlishvili, V. K. Dugaev, A. Ernst, I. V. Maznichenko, N. Arnold, C. Jia, J. Berakdar, I. Mertig, and J. Barnaś, The optical tweezer of skyrmions, npj Comput. Mater. **6**, 140 (2020).
[4] J. Graf, H. Pfeifer, F. Marquardt, and S. Viola Kusminskiy, Cavity optomagnonics with magnetic textures: Coupling a magnetic vortex to light, Phys. Rev. B **98**, 241406(R) (2018).
[5] A. Osada, A. Gloppe, R. Hisatomi, A. Noguchi, R. Yamazaki, M. Nomura, Y. Nakamura, and K. Usami, Brillouin Light Scattering by Magnetic Quasivortices in Cavity Optomagnonics, Phys. Rev. Lett. **120**, 133602 (2018).
[6] C. W. Sandweg, Y. Kajiwara, A. V. Chumak, A. A. Serga, V. I. Vasyuchka, M. B. Jungfleisch, E. Saitoh, and B. Hillebrands, Spin Pumping by Parametrically Excited Exchange Magnons, Phys. Rev. Lett. **106**, 216601 (2011).
[7] F. D. Czeschka, L. Dreher, M. S. Brandt, M. Weiler, M. Althammer, I.-M. Imort, G. Reiss, A. Thomas, W. Schoch, W. Limmer, H. Huebl, R. Gross, and S. T. B. Goennenwein, Scaling Behavior of the Spin Pumping Effect in Ferromagnet-Platinum Bilayers, Phys. Rev. Lett. **107**, 046601 (2011).
[8] B. Heinrich, C. Burrowes, E. Montoya, B. Kardasz, E. Girt, Y. Y. Song, Y. Y. Sun, and M. Z. Wu, Spin Pumping at the Magnetic Insulator (YIG)/Normal Metal (Au) Interfaces, Phys. Rev. Lett. **107**, 066604 (2011).
[9] Y. Shiomi, J. Lustikova, S. Watanabe, D. Hirobe, S. Takahashi, and E. Saitoh, Spin pumping from nuclear spin waves, Nat. Phys. **15**, 22 (2019).
[10] X. F. Zhang, C. L. Zou, L. Jiang, and H. X. Tang, Strongly Coupled Magnons and Cavity Microwave Photons, Phys. Rev. Lett. **113**, 156401 (2014).
[11] M. Harder, Y. Yang, B. M. Yao, C. H. Yu, J. W. Rao, Y. S. Gui, R. L. Stamps, and C. M. Hu, Level Attraction Due to Dissipative Magnon-Photon Coupling, Phys. Rev. Lett. **121**, 137203 (2018).
[12] Y. Tabuchi, S. Ishino, A. Noguchi, T. Ishikawa, R. Yamazaki, K. Usami, and Y. Nakamura, Coherent coupling between a ferromagnetic magnon and a superconducting qubit, Science **349**, 405 (2015).
[13] D. Lachance-Quirion, S. P. Wolski, Y. Tabuchi, S. Kono, K. Usami, and Y. Nakamura, Entanglement-based single-shot

detection of a single magnon with a superconducting qubit, Science **367**, 425 (2020).
[14] W. Cai, J. Han, F. Mei, Y. Xu, Y. Ma, X. Li, H. Wang, Y. P. Song, Z. Y. Xue, Z. Q. Yin, S. Jia, and L. Sun, Observation of Topological Magnon Insulator States in a Superconducting Circuit, Phys. Rev. Lett. **123**, 080501 (2019).
[15] J. Li, S. Y. Zhu, and G. S. Agarwal, Magnon-Photon-Phonon Entanglement in Cavity Magnomechanics, Phys. Rev. Lett. **121**, 203601 (2018).
[16] C. A. Potts, V. A. S. V. Bittencourt, S. V. Kusminskiy, and J. P. Davis, Magnon-Phonon Quantum Correlation Thermometry, Phys. Rev. Appl. **13**, 064001 (2020).
[17] X. F. Zhang, C. L. Zou, L. Jiang, and H. X. Tang, Cavity magnomechanics, Sci. Adv. **2**, e1501286 (2016).
[18] Y. S. Cao, P. Yan, H. Huebl, S. T. B. Goennenwein, and G. E. W. Bauer, Exchange magnon-polaritons in microwave cavities, Phys. Rev. B **91**, 094423 (2015).
[19] V. V. Kruglyak, S. O. Demokritov, and D. Grundler, Magnonics, J. Phys. D: Appl. Phys. **43**, 260301 (2010).
[20] D. K. Zhang, X. M. Wang, T. F. Li, X. Q. Luo, W. D. Wu, F. Nori, and J. Q. You, Cavity quantum electrodynamics with ferromagnetic magnons in a small yttrium-iron-garnet sphere, npj Quantum Inf. **1**, 15014 (2015).
[21] I. Boventer, M. Pfirrmann, J. Krause, Y. Schön, M. Kläui, and M. Weides, Complex temperature dependence of coupling and dissipation of cavity magnon polaritons from millikelvin to room temperature, Phys. Rev. B **97**, 184420 (2018).
[22] X. F. Zhang, C. L. Zou, N. Zhu, F. Marquardt, L. Jiang, and H. X. Tang, Magnon dark modes and gradient memory, Nat. Commun. **6**, 8914 (2015).
[23] C. W. Zollitsch, K. Mueller, D. P. Franke, S. T. B. Goennenwein, M. S. Brandt, R. Gross, and H. Huebl, High cooperativity coupling between a phosphorus donor spin ensemble and a superconducting microwave resonator, Appl. Phys. Lett. **107**, 142105 (2015).
[24] L. Bai, M. Harder, Y. P. Chen, X. Fan, J. Q. Xiao, and C. M. Hu, Spin Pumping in Electrodynamically Coupled Magnon-Photon Systems, Phys. Rev. Lett. **114**, 227201 (2015).
[25] L. H. Bai, M. Harder, P. Hyde, Z. Zhang, C. M. Hu, Y. P. Chen, and J. Q. Xiao, Cavity Mediated Manipulation of Distant Spin Currents Using a Cavity-Magnon-Polariton, Phys. Rev. Lett. **118**, 217201 (2017).
[26] H. Y. Yuan, Y. S. Cao, A. Kamra, R. A. Duine, and P. Yan, Quantum magnonics: When magnon spintronics meets quantum information science, Phys. Rep. **965**, 1 (2022).
[27] Y. P. Wang, G. Q. Zhang, D. k. Zhang, T. F. Li, C. M. Hu, and J. Q. You, Bistability of Cavity Magnon Polaritons, Phys. Rev. Lett. **120**, 057202 (2018).
[28] G. Q. Zhang, Y. P. Wang, and J. Q. You, Theory of the magnon Kerr effect in cavity magnonics, Sci. China Phys. Mech. Astron. **62**, 987511 (2019).
[29] C. Z. Chai, X. X. Hu, C. L. Zou, G. C. Guo, and C. H. Dong, Thermal bistability of magnon in yttrium iron garnet microspheres, Appl. Phys. Lett. **114**, 021101 (2019).
[30] Y. Xiao, X. H. Yan, Y. Zhang, V. L. Grigoryan, C. M. Hu, H. Guo, and K. Xia, Magnon dark mode of an antiferromagnetic insulator in a microwave cavity, Phys. Rev. B **99**, 094407 (2019).
[31] C. Kong, B. Wang, Z. X. Liu, H. Xiong, and Y. Wu, Magnetically controllable slow light based on magnetostrictive forces, Opt. Express **27**, 5544 (2019).
[32] J. Zhao, L. H. Wu, T. F. Li, Y. X. Liu, F. Nori, Y. L. Liu, and J. F. Du, Phase-Controlled Pathway Interferences and Switchable Fast-Slow Light in a Cavity-Magnon Polariton System, Phys. Rev. Appl. **15**, 024056 (2021).
[33] B. Wang, Z. X. Liu, C. Kong, H. Xiong, and Y. Wu, Magnon-induced transparency and amplification in $\mathcal{PT}$-symmetric cavity-magnon system, Opt. Express **26**, 20248 (2018).
[34] K. Ullah, M. T. Naseem, and Ö. E. Müstecaplıoğlu, Tunable multiwindow magnomechanically induced transparency, Fano resonances, and slow-to-fast light conversion, Phys. Rev. A **102**, 033721 (2020).
[35] Z. D. Zhang, M. O. Scully, and G. S. Agarwal, Quantum entanglement between two magnon modes via Kerr nonlinearity driven far from equilibrium, Phys. Rev. Res. **1**, 023021 (2019).
[36] M. Yu, H. Shen, and J. Li, Magnetostrictively Induced Stationary Entanglement between Two Microwave Fields, Phys. Rev. Lett. **124**, 213604 (2020).
[37] J. M. P. Nair and G. S. Agarwal, Deterministic quantum entanglement between macroscopic ferrite samples, Appl. Phys. Lett. **117**, 084001 (2020).
[38] B. Hussain, S. Qamar, and M. Irfan, Entanglement enhancement in cavity magnomechanics by an optical parametric amplifier, Phys. Rev. A **105**, 063704 (2022).
[39] J. Li, S. Y. Zhu, and G. S. Agarwal, Squeezed states of magnons and phonons in cavity magnomechanics, Phys. Rev. A **99**, 021801(R) (2019).
[40] A. L. Pankratov, K. G. Fedorov, M. Salerno, S. V. Shitov, and A. V. Ustinov, Nonreciprocal transmission of microwaves through a long Josephson junction, Phys. Rev. B **92**, 104501 (2015).
[41] F. Trojánek, K. Žídek, B. Dzurňák, M. Kozák, and P. Malý, Nonlinear optical properties of nanocrystalline diamond, Opt. Express **18**, 1349 (2010).
[42] C. Schriever, F. Bianco, M. Cazzanelli, M. Ghulinyan, C. Eisenschmidt, J. de Boor, A. Schmid, J. Heitmann, L. Pavesi, and J. Schilling, Second-order optical nonlinearity in silicon waveguides: Inhomogeneous stress and interfaces, Adv. Opt. Mater. **3**, 129 (2015).
[43] A. F. Borghesani, C. Braggio, and G. Carugno, Generation of microwave radiation by nonlinear interaction of a high-power, high-repetition rate, 1064 nm laser in $KTiOPO_4$ crystals, Opt. Lett. **38**, 4465 (2013).
[44] A. F. Borghesani, C. Braggio, and M. Guarise, Microwave emission by nonlinear crystals irradiated with a high-intensity, mode-locked laser, J. Opt. **18**, 065503 (2016).
[45] K.-W. Huang, Y. Wu, and L.-G. Si, Parametric-amplification-induced nonreciprocal magnon laser, Opt. Lett. **47**, 3311 (2022).
[46] E. Nitiss, J. Q. Hu, A. Stroganov, and C. S. Brès, Optically reconfigurable quasi-phase-matching in silicon nitride microresonators, Nat. Photonics **16**, 134 (2022).
[47] X. Guo, C. L. Zou, and H. X. Tang, Second-harmonic generation in aluminum nitride microrings with 2500%/W conversion efficiency, Optica **3**, 1126 (2016).
[48] C. K. Law, Effective Hamiltonian for the radiation in a cavity with a moving mirror and a time-varying dielectric medium, Phys. Rev. A **49**, 433 (1994).

[49] M. Fernandez-Serra, Fifty years of the dynamical Casimir effect, Physics **2**, 67 (2009).
[50] S. Tanaka and K. Kanki, The dynamical Casimir effect in a dissipative optomechanical cavity interacting with photonic crystal, Physics **2**, 34 (2020).
[51] V. Macrì, A. Ridolfo, O. Di Stefano, A. F. Kockum, F. Nori, and S. Savasta, Nonperturbative Dynamical Casimir Effect in Optomechanical Systems: Vacuum Casimir-Rabi Splittings, Phys. Rev. X **8**, 011031 (2018).
[52] H. Huebl, C. W. Zollitsch, J. Lotze, F. Hocke, M. Greifenstein, A. Marx, R. Gross, and S. T. B. Goennenwein, High Cooperativity in Coupled Microwave Resonator Ferrimagnetic Insulator Hybrids, Phys. Rev. Lett. **111**, 127003 (2013).
[53] Y. Tabuchi, S. Ishino, T. Ishikawa, R. Yamazaki, K. Usami, and Y. Nakamura, Hybridizing Ferromagnetic Magnons and Microwave Photons in the Quantum Limit, Phys. Rev. Lett. **113**, 083603 (2014).
[54] M. Goryachev, W. G. Farr, D. L. Creedon, Y. Fan, M. Kostylev, and M. E. Tobar, High-Cooperativity Cavity QED with Magnons at Microwave Frequencies, Phys. Rev. Appl. **2**, 054002 (2014).
[55] P. Forn-Díaz, L. Lamata, E. Rico, J. Kono, and E. Solano, Ultrastrong coupling regimes of light-matter interaction, Rev. Mod. Phys. **91**, 025005 (2019).
[56] T. Holstein and H. Primakoff, Field dependence of the intrinsic domain magnetization of a ferromagnet, Phys. Rev. **58**, 1098 (1940).
[57] Y. P. Wang, G. Q. Zhang, D. Zhang, X. Q. Luo, W. Xiong, S. P. Wang, T. F. Li, C. M. Hu, and J. Q. You, Magnon Kerr effect in a strongly coupled cavity-magnon system, Phys. Rev. B **94**, 224410 (2016).
[58] D. Walls and G. J. Milburn, *Quantum Optics* (Springer, Berlin, 2008).
[59] The Hamiltonian of this nonlinear pumping term should be $\chi^{(2)}(d^\dagger a^2 + d a^{\dagger 2})$, where $\chi^{(2)}$ is the second-order susceptibility and $d^\dagger(d)$ gives the creation (annihilation) operator for the pump field. For a strong pump field, one can treat it as a classical field and hence derive $G = \chi^{(2)}\langle d\rangle$ (see Chap. 5 in Ref. [58] for details).
[60] I. Breunig, Three-wave mixing in whispering gallery resonators, Laser Photonics Rev. **10**, 569 (2016).
[61] C. W. Gardiner and P. Zoller, *Quantum Noise* (Springer, Berlin, 2000).
[62] Y. Li, V. G. Yefremenko, M. Lisovenko, C. Trevillian, T. Polakovic, T. W. Cecil, P. S. Barry, J. Pearson, R. Divan, V. Tyberkevych, C. L. Chang, U. Welp, W.-K. Kwok, and V. Novosad, Coherent Coupling of Two Remote Magnonic Resonators Mediated by Superconducting Circuits, Phys. Rev. Lett. **128**, 047701 (2022).
[63] D. Vitali, P. Tombesi, M. J. Woolley, A. C. Doherty, and G. J. Milburn, Entangling a nanomechanical resonator and a superconducting microwave cavity, Phys. Rev. A **76**, 042336 (2007).
[64] P. C. Parks and V. Hahn, *Stability Theory* (Springer, New York, 1993).
[65] G. Vidal and R. F. Werner, Computable measure of entanglement, Phys. Rev. A **65**, 032314 (2002).
[66] M. B. Plenio, Logarithmic Negativity: A Full Entanglement Monotone That is not Convex, Phys. Rev. Lett. **95**, 090503 (2005).
[67] J. Li and S. Y. Zhu, Entangling two magnon modes via magnetostrictive interaction, New J. Phys. **21**, 085001 (2019).
[68] G. Adesso and F. Illuminati, Continuous variable tangle, monogamy inequality, and entanglement sharing in Gaussian states of continuous variable systems, New J. Phys. **8**, 15 (2006).
[69] G. Adesso and F. Illuminati, Entanglement in continuous variable systems: Recent advances and current perspectives, J. Phys. A: Math. Theor. **40**, 7821 (2007).
[70] This condition implies $\delta_{m_1}, \delta_{m_2} \neq 0$ for a nonzero coupling strength g.